Fluorine assembly nanocluster breaks the shackles of immunosuppression to turn the cold tumor hot

Zhaoting Li[a,1], Lianghan Zhu[a,1], Honghao Sun[a], Yuexin Shen[a], Dandan Hu[a], Wenhao Wu[a], Yixin Wang[a], Chenggen Qian[a], and Minjie Sun[a,2]

[a]State Key Laboratory of Natural Medicines, Department of Pharmaceutics, China Pharmaceutical University, Nanjing 210009, China

Edited by Chad A. Mirkin, Northwestern University, Evanston, IL, and approved November 10, 2020 (received for review June 3, 2020)

Clinical investigations have shown that a nonimmunogenic "cold" tumor is usually accompanied by few immunopositive cells and more immunosuppressive cells in the tumor microenvironment (TME), which is still the bottleneck of immune activation. Here, a fluorine assembly nanocluster was explored to break the shackles of immunosuppression, reawaken the immune system, and turn the cold tumor "hot." Once under laser irradiation, FS@PMPt produces sufficient reactive oxygen species (ROS) to fracture the ROS-sensitive linker, thus releasing the cisplatin conjugated PMPt to penetrate into the tumors and kill the regulatory T cells (Tregs) and myeloid-derived suppressor cells (MDSCs). Meanwhile, ROS will induce potent immunogenic cell death (ICD) and further promote the accumulation of dendritic cells (DCs) and T cells, therefore not only increasing the infiltration of immunopositive cells from the outside but also reducing the immunosuppressive cells from the inside to break through the bottleneck of immune activation. The FS@PMPt nanocluster regulates the immune process in TME from negative to positive, from shallow to deep, to turn the cold tumor into a hot tumor and provoke a robust antitumor immune response.

photodynamic immunotherapy | immunosuppressive tumor microenvironment | cold tumor | immunogenic cell death | nanocluster

In recent years, with the development of tumor immunology research, some scholars put forward the concept of "cold" and "hot" tumors to lead the future of antitumor immune research. In this concept, the number of tumor-infiltrating lymphocytes is taken as the scoring standard, and the tumor with more T cells and other positive immunoregulatory cells is called a hot tumor. On the contrary, a tumor with fewer or no positive immunoregulatory cells and more immunosuppressive cells is called a cold tumor (1–3). Cold tumors are usually unrecognized by the immune system for various reasons and do not cause an effective immune response. In general, antigen-presenting cells (APCs) can no longer recognize such tumors, and T cells have been excluded from the tumor microenvironment (TME), which causes a huge obstacle for antitumor immunotherapy (4, 5). Clinical investigations point out that most tumors are cold, and regulating the immune process to turn a cold tumor into a hot tumor has become an urgent task of antitumor immunotherapy.

Photodynamic therapy (PDT) could generate immunogenic cell death (ICD), accompanied by the release of high-mobility group box 1 protein (HMGB1) and adenosine triphosphate (ATP) and the exposure of calreticulin (CRT), sending the "eat-me" signal and promoting the antigen presentation and maturation of dendritic cells (DCs) (6, 7). ICD could recruit the DCs and antigen-specific cytotoxic T lymphocytes (CTLs) to the TME, thus turning the cold tumor into a hot tumor and activating the antitumor immune response. Also, for the photodynamic immunotherapy, most researchers focus on developing more effective PDT strategies to provoke robust antitumor immune responses. Encouragingly, they have made remarkable progress in increasing the tumor infiltration of immunopositive regulatory cells, such as DCs and CTLs (8–10). However, the immunosuppressive TME of the cold tumor is known to impair the function of DCs and CTLs to greatly diminish the efficacy of the photodynamic immunotherapy. Notably, regulatory T cells (Tregs), supporting the establishment of an immunosuppressive TME, suppress T cell immune responses and activities of APCs, including DCs and macrophages, through several mechanisms. Tregs inhibit the expression of CD80 and CD86 via the cytotoxic T lymphocyte associated protein 4 (CTLA-4), which will directly compromise the ICD-induced APC maturation and activation. More lethally, Tregs can promote the apoptosis of effector T cells in the TME through cell to cell contact and interleukin-2 (IL-2) deprivation (11–13). In addition, Tregs could inhibit the immunostimulatory functions of DCs and infiltration of effector T cells by producing transforming growth factor-β (TGF-β) and IL-10. Interestingly, TGF-β can further lead to the differentiation of naive $CD4^+$ T cells into Tregs and promote the Tregs accumulation in tumors (14–17). Similarly, myeloid-derived suppressor cells (MDSCs) can also recruit Tregs and promote their proliferation by secreting IL-10 and TGF-β. MDSCs, working hand in glove with Tregs, jointly maintain the immunosuppression of TME, prevent cold tumors from becoming hot, and greatly reduce the efficacy of photodynamic immunotherapy (18, 19). It is therefore of the utmost importance that we break the shackles of immunosuppression in the TME to turn a cold tumor into a hot tumor from the perspective of immune regulation.

There is sufficient evidence to support that some chemotherapeutic drugs with a certain dosage, such as paclitaxel and cisplatin, are capable of decreasing the MDSCs and Tregs to regulate the immunosuppressive TME (20–24). Here, as shown

Significance

"Cold" tumors are good at camouflaging themselves, thus making it difficult for the immune system to recognize and to construct a great barrier for cancer immunotherapies. New methods that could awaken the immune system, enhance T cells and antigen-presenting cells (APCs) trafficking, and relieve immunosuppression to treat cold tumors are urgently in need. Here, we first report a chemically ingenious nanocluster FS@PMPt assembly by fluorine–fluorine interaction to regulate the immune process. The nanocluster not only increased the infiltration of immunopositive cells from the outside but also decreased the immunosuppressive cells from the inside to break the shackles of immunosuppression, which provides a promising paradigm for improving the anti–cold tumor immunotherapy.

Author contributions: Z.L. and M.S. designed research; Z.L., L.Z., H.S., Y.S., D.H., W.W., and Y.W. performed research; Z.L. and L.Z. contributed new reagents/analytic tools; Z.L., L.Z., H.S., Y.S., Y.W., and C.Q. analyzed data; and Z.L. and M.S. wrote the paper.

The authors declare no competing interest.

This article is a PNAS Direct Submission.

[1]Z.L. and L.Z. contributed equally to this work.

[2]To whom correspondence may be addressed. Email: msun@cpu.edu.cn.

This article contains supporting information online at https://www.pnas.org/lookup/suppl/doi:10.1073/pnas.2011297117/-/DCSupplemental.

First published December 14, 2020.

in Fig. 1*A*, a fluorinated cisplatin drug carrier (F-S-PAMAM-Pt) and a fluorinated photosensitizer chlorine e6 (Ce6) copolymer (F-Ce6-PEG) were synthesized, and they can assemble with perfluorocarbon (PFC) through fluorine–fluorine (F–F) interaction to form the nanocluster FS@PMPt. The nanocluster has good stability because of the F–F interaction and PEG protection. Also, after pressing the Ce6 start key through laser irradiation, oxygen contained in PFC can ensure the production of enough reactive oxygen species (ROS), thus triggering a strong ICD-induced immune response and increasing the infiltration of DCs and $CD8^+$ T cells to make the cold tumor become hot. Meanwhile, the ROS will break the ROS-sensitive bond and release the cisplatin conjugated PMPt to penetrate into the tumor to kill the intratumoral Tregs and MDSCs, which are the culprit of the cold tumor, thus breaking the shackles of immunosuppression to further enhance the photodynamic immunotherapy (Fig. 1*B*).

Results

Preparation and Characterization of the Nanoclusters. To prepare the FS@PMPt nanocluster, first, the ROS-sensitive F-S-PAMAM-Pt (*SI Appendix*, Figs. S1 and S4), non-ROS-sensitive F-*N*-PAMAM-Pt (*SI Appendix*, Figs. S2 and S5), and F-Ce6-PEG (*SI Appendix*, Figs. S3 and S6) were synthesized. Then the F-S-PAMAM-Pt, PFC, and F-Ce6-PEG were assembled into FS@PMPt through F–F interaction, with the F-S-PAMAM-Pt clustered on the surface of the PFC core. It was shown that the ROS-sensitive FS@PMPt is spherical in shape (Fig. 2*A*), with a particle size of ∼165 nm and a zeta potential of ∼18 mv, similar to those of the non-ROS-sensitive FN@PMPt (Fig. 2*B*). Due to the strong force of F–F interaction and the protection of PEG, both the FS@PMPt and the FN@PMPt showed good colloidal stability (Fig. 2*C*). As shown in the drug release assay in Fig. 2*D*, in the absence of laser irradiation, the release of cisplatin prodrugs in the ROS-sensitive FS@PMPt is very slow. Once under laser irradiation, the release of cisplatin prodrugs in the ROS sensitive FS@PMPt becomes much faster than that of the non-ROS-sensitive FN@PMPt. Also, we found that the FS@PMPt and FN@PMPt both showed superior oxygen carrying and ROS generating abilities because of the excellent properties of PFC to dissolve oxygen (Fig. 2*E* and *SI Appendix*, Fig. S7).

Antitumor Efficacy In Vitro. In order to detect the cell uptake of the PMPt prodrugs in 4T1 cells, fluoresceine isothiocyanate (FITC) was conjugated on the amino end of the PMPt, and the flow cytometry assay was performed. As shown in Fig. 3*A*, the fluorescence intensity in the FS@PMPt + L group was stronger than that of FN@PMPt + L and FS@PMPt groups, suggesting that the PMPt prodrugs in the ROS-sensitive FS@PMPt nanocluster

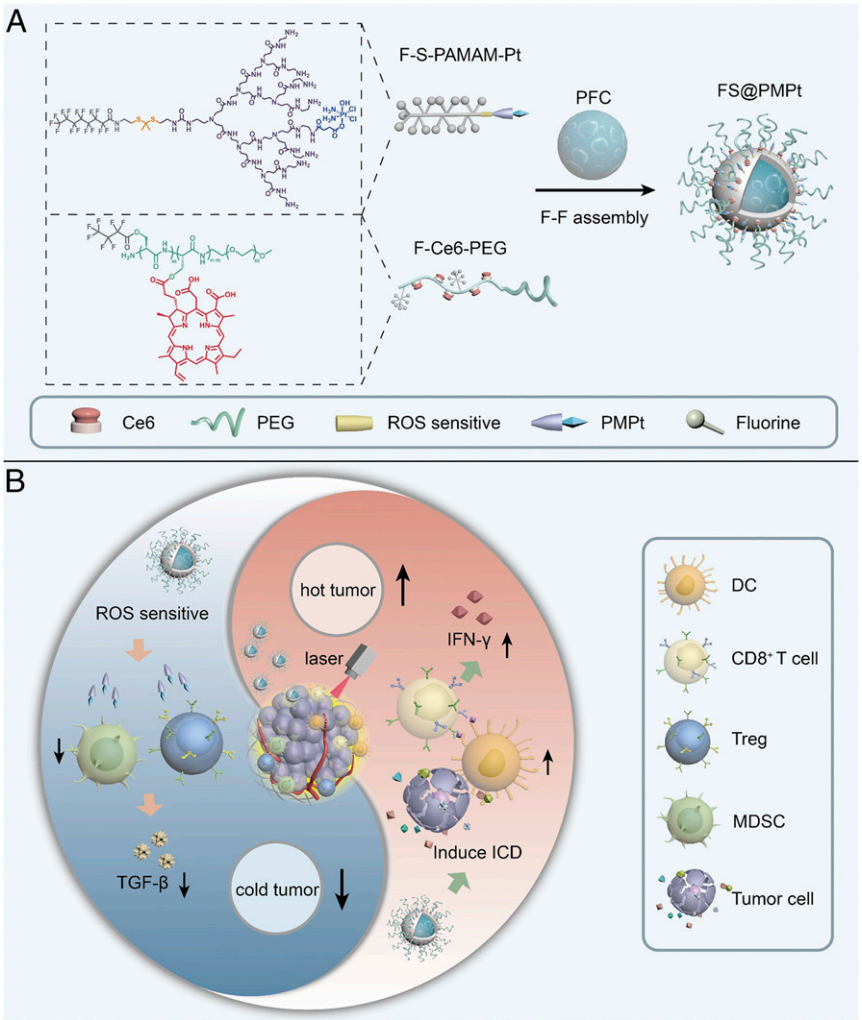

Fig. 1. Preparation and immunoregulation of FS@PMPt. (*A*) Chemical structures of F-S-PAMAM-Pt and F-Ce6-PEG and preparation of the FS@PMPt nanocluster. (*B*) Schematic illustration of the working mechanism of the nanocluster FS@PMPt on turning a cold tumor into a hot tumor.

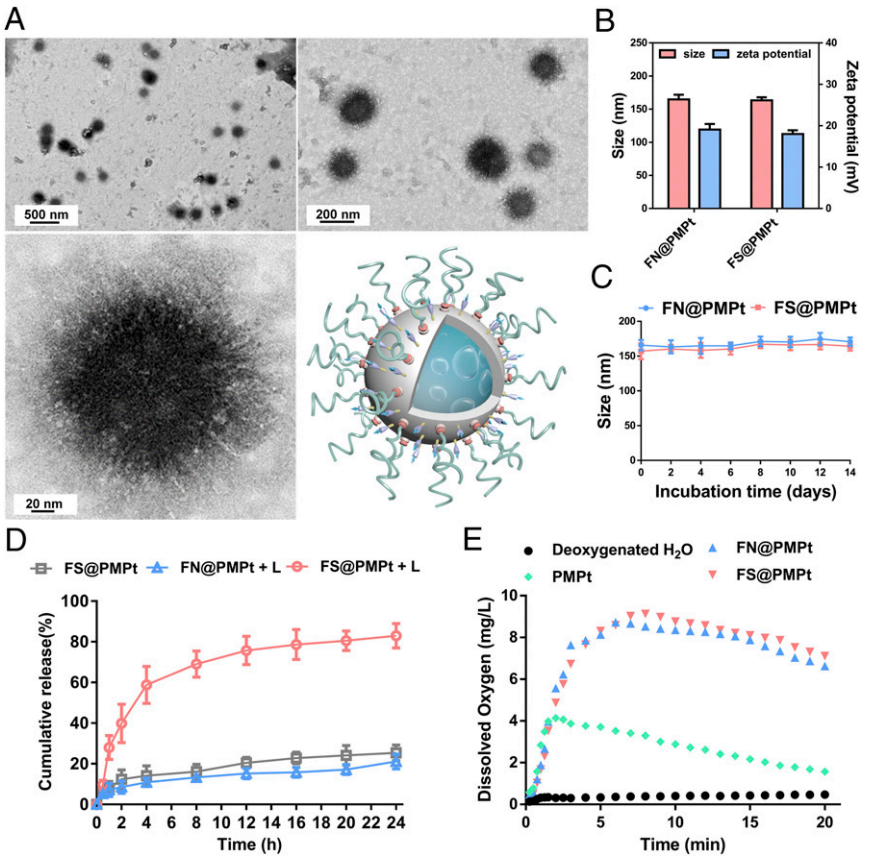

Fig. 2. Physicochemical characterization of the nanoclusters. (*A*) Transmission electron microscopy (TEM) images of FS@PMPt. (*B*) Hydrodynamic size and zeta potential of FS@PMPt and FN@PMPt. (*C*) Colloidal stability of FS@PMPt and FN@PMPt in 10% fetal bovine serum (FBS) solution. (*D*) In vitro drug release of FS@PMPt and FN@PMPt with or without the trigger of a laser (+L). Results are expressed as mean ± SD ($n = 3$). (*E*) Time-dependent changes of dissolved oxygen concentrations in deoxygenated pure water without or with addition of oxygen-loaded nanoclusters.

could enter the cells more effectively under the trigger of laser irradiation (+L). Furthermore, we established a three-dimensional (3D) tumor sphere model of 4T1 cells to verify the deep penetration ability of the nanoclusters. According to the confocal microscopic Z-stack imaging, FS@PMPt showed poor permeability in vitro because of its larger particle size and PEG package, while once triggered by a laser, the deep penetration ability is significantly enhanced, and strong FITC fluorescence can be detected even at a depth of 60 μm (Fig. 3*B* and *SI Appendix*, Fig. S8). Both drug intake and penetration are for the purpose of achieving potent antitumor efficacy. The cell viability of 4T1 cells treated with FS@PMPt was about 75%, while under the trigger of laser irradiation, cell viability decreased to 17%, significantly lower than that in the FN@PMPt + L group (Fig. 3*C*). Consistent with the inhibition of cell proliferation, FS@PMPt + L treatment induced more apoptosis of 4T1 cells than the FN@PMPt + L and PMPt treatment (Fig. 3*D*). PFCs have excellent biosafety and oxygen-carrying capacity and are often used as an outstanding type of artificial blood substitute (25, 26). In addition, sufficient oxygen-carrying capacity can ensure enough ROS generation through photodynamic therapy, thus promoting potent ICD-induced immune activation. Therefore, the ROS production was tested by flow cytometry assay. As shown in Fig. 3*E*, the FN@PMPt and FS@PMPt exhibited powerful ROS generation ability under laser irradiation, almost equivalent to the positive control. This ensures the ROS-sensitive release of the PMPt prodrugs and further tumor penetration.

Immune Activation In Vitro. The primary feature of ICD is the increased expression of CRT, sending the eat-me signal to further activate the APCs (27, 28). We used both confocal observation and flow cytometry assay to explore the CRT exposure in 4T1 cells after different treatments. As shown in Fig. 4*A*, the CRT expression in 4T1 cells of the phosphate buffer saline (PBS) group was very low. In the PMPt or FS@PMPt group, there was little increase of CRT expression according to the confocal images. However, after the FN@PMPt + L or FS@PMPt + L treatment, significantly more CRT exposure was observed. Similarly, according to the results of flow cytometry assay in Fig. 4 *B* and *C*, the CRT expression increased from 1.4 to 46.1% after the FS@PMPt + L treatment and 43.5% after the FN@PMPt + L treatment. It was supposed that CRT exposure is mainly caused by the generated ROS under laser irradiation. Also, ATP and HMGB1 secretion was detected, and we found that the FS@PMPt treatment could moderately increase ATP and HMGB1 concentration in the 4T1 cell supernatant (Fig. 4 *D* and *E*). Once under laser irradiation, the ATP level in FS@PMPt + L group exhibited a 3.6-fold up-regulation, and the HMGB1 level increased about 3 times, indicating a significantly enhanced ICD effect. Furthermore, the CD40 and CD86 expression on DCs was tested by flow cytometry assay. As shown in Fig. 4*F*, there were only ~22.9% mature DCs in the PBS-treated group. Meanwhile, a slight increase was observed in the PMPt group (32.6%) and the FS@PMPt group (29.6%). Notably, after the FS@PMPt + L treatment, the proportion of mature DCs reached 53.4%, demonstrating an obvious activated ICD-induced immune process. Taken together, the FS@PMPt + L

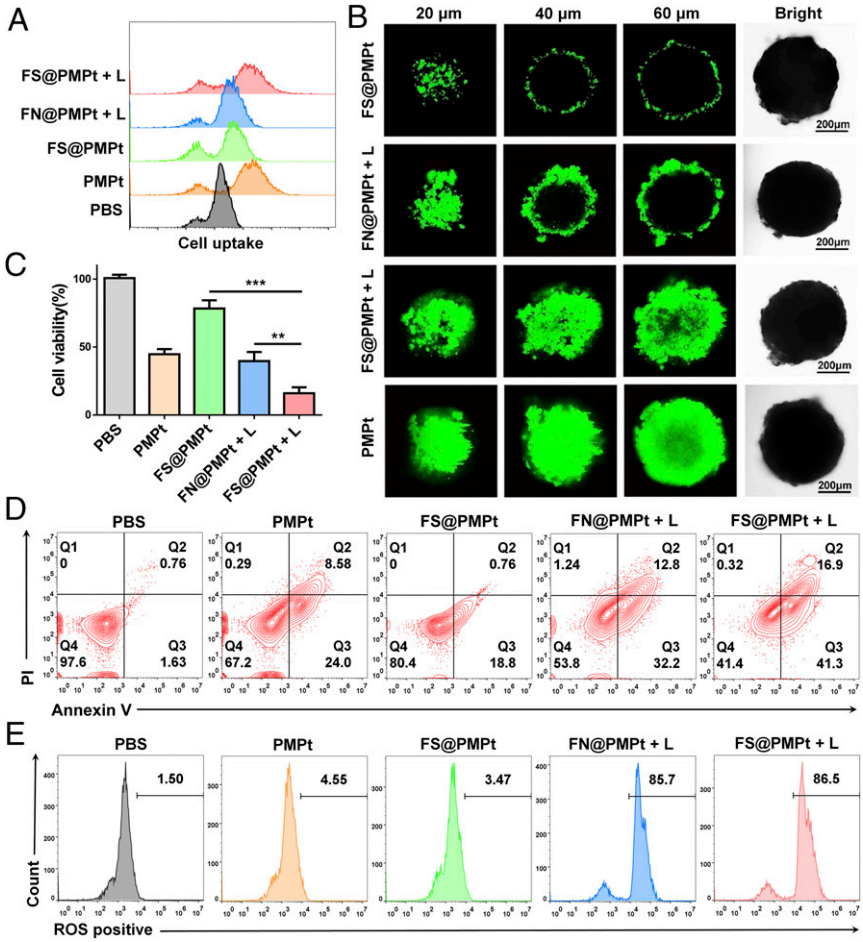

Fig. 3. Antitumor efficacy in vitro. (*A*) Cell uptake analyzed by flow cytometry after different treatments with the nanoclusters. (*B*) Representative Z-stack confocal images of the 3D 4T1 tumor spheroids after different treatments with the nanoclusters for 12 h. (*C*) Cell viability and (*D*) apoptosis assay of 4T1 cells after different treatments with the nanoclusters. *P* values were calculated by Student's *t* test, $^{**}P < 0.01$, $^{***}P < 0.001$. (*E*) ROS generation detected by the flow cytometry assay after different treatments of the nanoclusters.

treatment could increase the CRT expression and induce the secretion of ATP and HMGB1 to generate an ICD effect and further promote the antigen presentation and maturation of DCs to regulate the immune process.

Antitumor Efficacy In Vivo. The antitumor efficacy of the nanoclusters was evaluated in a 4T1 orthotopic tumor model. When the tumor volumes reached ~100 mm^3, the mice were divided into five groups: saline, PMPt, FS@PMPt, FN@PMPt + L, and FS@PMPt + L, and the laser irradiation was conducted at 6 h after intravenous (i.v.) injection. Also, the tumor volumes were recorded every other day. As shown in Fig. 5*A*, FS@PMPt exhibited better antitumor efficacy than PMPt. This is partly due to the good stability of FS@PMPt, which can ensure their transportation in blood circulation and help the nanoclusters reach the tumor focus (29). Notably, the FS@PMPt + L treatment showed the best tumor growth inhibition, and the tumor volumes were significantly reduced (Fig. 5*B*). As expected, the mean tumor weight in the FS@PMPt + L group was lighter than that in FN@PMPt + L, which was consistent with the tumors volumes, indicating the importance of the ROS-sensitive linker to release PMPt prodrugs for further penetration and immune regulation of the TME (Fig. 5*C*). The survival time is the final index to evaluate the antitumor effect. As shown in Fig. 5*D*, PMPt treatment only prolonged the median survival from 31 to 36 d. However, encouragingly, FS@PMPt + L treatment prolonged the median survival to 58.5 d, significantly better than the FN@PMPt + L (49 d) and FS@PMPt (40.5 d). From the hematoxylin-eosin (H&E) staining assay, the cell morphology of the tumors in the FS@PMPt + L group changed, and more necrosis was observed (Fig. 5*E*). In addition, the results of Ki67 immunohistochemical staining showed that FS@PMPt + L treatment inhibited the growth of tumor cells significantly better than FS@PMPt and FN@PMPt + L, in accordance with the growth curve of the tumor volumes. Furthermore, terminal deoxynucleotidyl transferase-mediated dUTP nick end labeling (TUNEL) staining showed a marked increase of green fluorescence in the FS@PMPt + L group, suggesting that the apoptotic rate of tumors in the FS@PMPt + L group was the highest (Fig. 5*E*).

In addition, antimetastasis experiments using a metastatic tumor model have been conducted to demonstrate the antitumor efficacy of immunity in living mice. As shown in *SI Appendix*, Fig. S9, the 4T1 metastatic breast cancer model in BALB/c mice was established. After different treatments, on day 30, the lungs were harvested for further analysis (*SI Appendix*, Fig. S9*A*). The number of metastatic nodules on the lung surface was significantly decreased after the FS@PMPt + L treatment, demonstrating that the nanocluster treatment can activate the immune systems to inhibit the lung metastasis (*SI Appendix*, Fig. S9*B*). Also, according to the lung images (*SI Appendix*, Fig. S9*C*) and H&E assay (*SI Appendix*, Fig. S9*D*), it

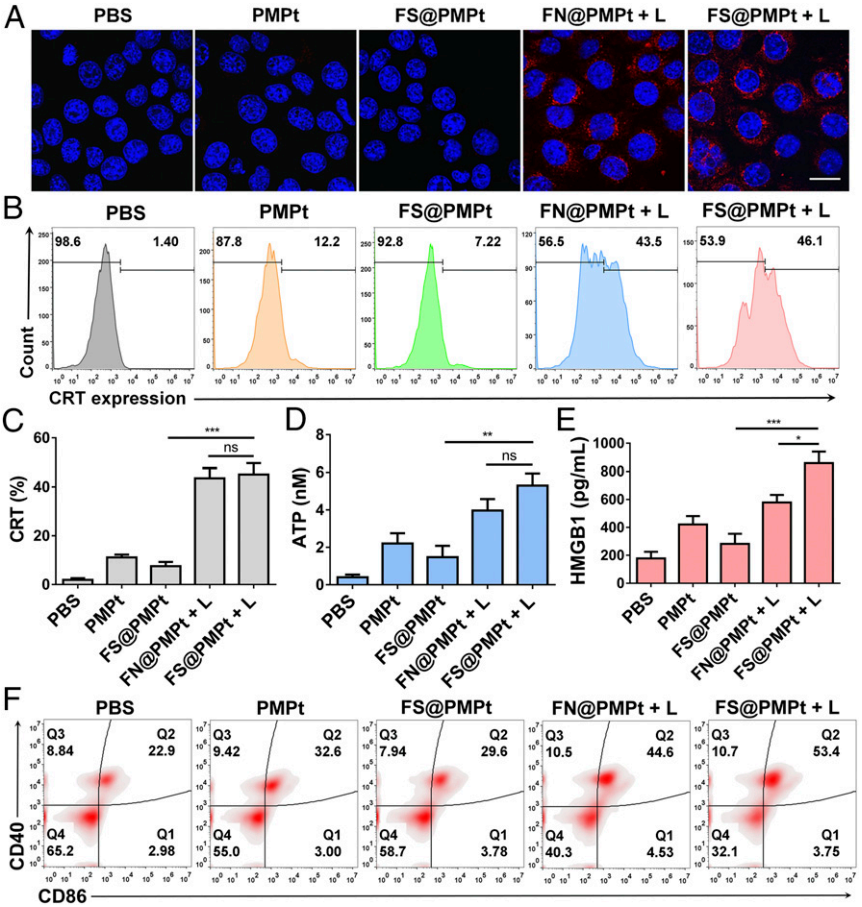

Fig. 4. Immune activation in vitro. (*A*) Confocal images of CRT exposure in 4T1 cells after different treatments with the nanoclusters. (*B*) Flow cytometry assay and (*C*) data analysis of the CRT expression in 4T1 cells after different treatments with the nanoclusters. (*D*) ATP and (*E*) HMGB1 in the cell supernatant detected by the ATP assay kit and enzyme-linked immunosorbent assay (ELISA). Results are shown as mean ± SD ($n = 3$); *P* values were calculated by Student's *t* test, $^{*}P < 0.05$, $^{**}P < 0.01$, $^{***}P < 0.001$, ns = no significant difference. (*F*) In vitro DC maturation ($CD40^{+}CD86^{+}$) detected by the flow cytometry assay after cocultured with 4T1 cells with different treatments.

was clearly shown that the treatment of FS@PMPt + L for orthotopic breast tumors could activate the immunity of the whole body, thereby exerting potent antimetastatic efficacy in the living mice.

Immune Activation In Vivo. DCs are the most important regulators of ICD immune response (30, 31). The CD40 and CD86 expression on $CD11c^{+}$ dendritic cells was detected by flow cytometry assay (Fig. 6 *A* and *B*). It was shown that FN@PMPt + L and FS@PMPt + L treatment could effectively up-regulate the CD40 and CD86 expression and thus promote the antigen presentation and maturation of DCs, which will further activate the T cells and enhance the $CD8^{+}$ T cell infiltration in the tumor. As shown in Fig. 6 *C* and *D*, after FS@PMPt + L treatment, the $CD8^{+}$ T cell infiltration increased from 17.8% (saline) to 40.9%, indicating the activated immune status in TME. However, the Tregs and MDSCs are the most typical immunosuppressive cells in the TME, which will greatly inhibit the immune function of the APCs and T cells (32, 33). Massive Treg infiltration was found in the saline group (40.9%), suggesting that the TME was in a cold tumor state of immunosuppression. Remarkably, Tregs were reduced to 7.54% in the FS@PMPt + L group (Fig. 6 *E* and *F*). Meanwhile, MDSCs were down-regulated to 12.1% after the treatment of FS@PMPt + L (Fig. 5 *G* and *H*). The decrease of Tregs and MDSCs demonstrates that the cold immunosuppressive tumor was turned to a hot immune activating status by the nanocluster. Also, compared with the cold tumor in the saline group, after the treatment with FS@PMPt + L, the $CD8^{+}$ to Treg ratio increased by 10.8 times, and the $CD4^{+}$ to Treg ratio increased by 2.5 times (Fig. 6 *I* and *J*). The nanocluster regulates the immune systems and helps the immune activated cells to take the initiative and become the dominant party in the TME. In addition, usually, the activation of an antitumor immune response is accompanied by the production of interferon-γ (IFN-γ), and the decrease of TGF-β expression often represents the attenuation of immunosuppression (34–36). As shown in Fig. 6 *K* and *L*, compared with the saline group, after the treatment with FS@PMPt + L, IFN-γ production showed a 4.4-fold increase, while TGF-β1 expression decreased by ~53%, further demonstrating the transformation from the immunosuppressive cold tumor to immune activated hot tumor.

Biosafety Evaluation In Vivo. Briefly, the healthy BALB/c mice ($n = 5$) were treated with saline, PMPt, FN@PMPt, and FS@PMPt by i.v. injection three times. Twenty-four hours after the last administration, the mice were euthanized, and the major organs were harvested for H&E staining. The blood serum was collected, and the levels of crucial hepatic and kidney function indicators, including alanine aminotransferase (ALT), aspartate aminotransferase (AST), and blood urine nitrogen (BUN), were tested following the manufacturer's instructions. As shown in *SI Appendix*, Fig. S10*A*, compared with the saline group, there was

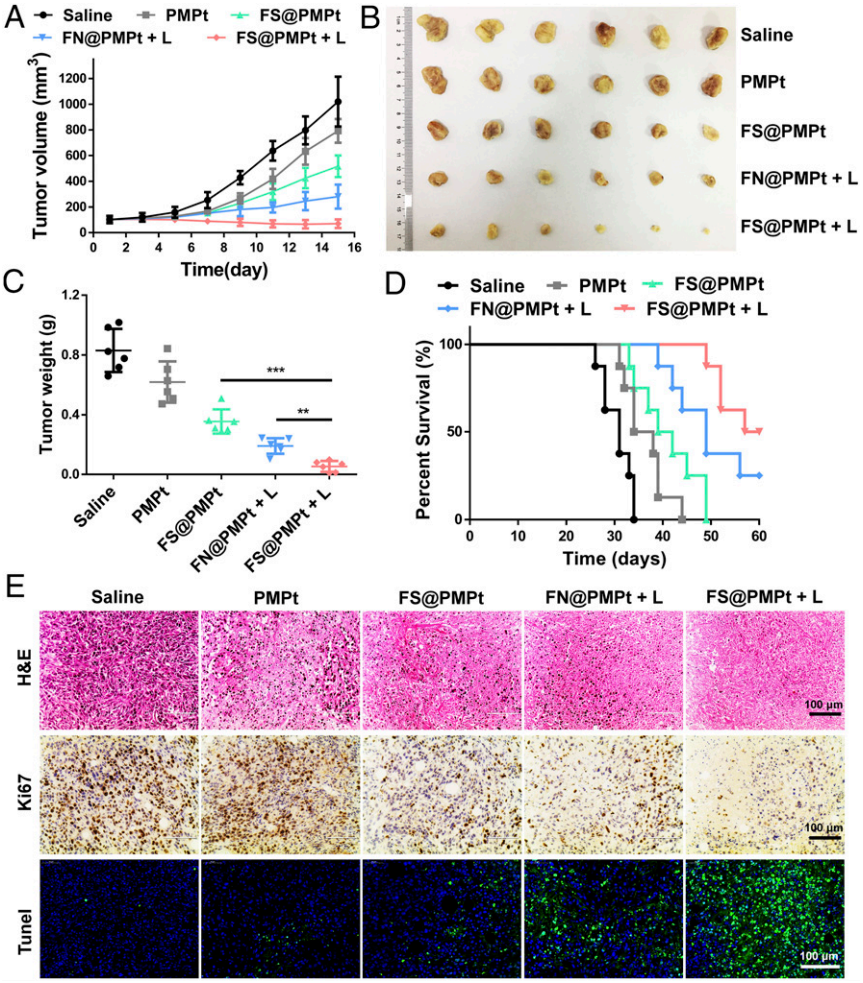

Fig. 5. Antitumor efficacy in vivo. (*A*) The 4T1 tumor growth curves after administration of saline, PMPt, FN@PMPt, and FS@PMPt with or without laser. (*B*) Images and (*C*) weight of the collected tumors ($n = 6$). *P* values were calculated by Student's *t* test, $^{**}P < 0.01$, $^{***}P < 0.001$. (*D*) Percent survival of 4T1 tumor-bearing mice after different treatments ($n = 8$). (*E*) Representative images of H&E staining, Ki67 immunohistochemistry staining, and TUNEL staining of the collected tumors with different treatments.

no significant physiological difference in the main tissues of the mice, and the histological sections of the heart, liver, spleen, lung, and kidney were normal after the treatment of the FS@PMPt nanoclusters. In addition, the ALT (*SI Appendix*, Fig. S10*B*), AST (*SI Appendix*, Fig. S10*C*), and BUN (*SI Appendix*, Fig. S10*D*) analysis of the blood serum indicated that the FS@PMPt treatment showed no obvious toxicity to the liver and kidney and had good in vivo biosafety.

Discussion

Immunotherapy has recently shifted the paradigm of cancer treatment; however, improvement of the response rate and reduction in cold tumors remains a tough challenge (37). For cancer patients, the immune system can detect and attack hot tumors, but it is indifferent to cold tumors. Cold tumors are usually good at camouflage and hide their antigens, constructing an immunosuppressvie TME, so that they are not recognized by APCs and escape the attack of effector T cells (1, 5). Therefore, anticancer immunotherapies that could convert immunosuppressive cold tumors into immunoactivated hot tumors are being sought.

To drive the remission of immunologically cold tumors, the first step is to help the immune system reestablish immune surveillance. One effective strategy is to generate ICD to release antigens inside the tumor and send the eat-me signal, which will further recruit DCs to the TME. DCs play the role of recognition in antitumor immune response and are responsible for presenting tumor antigens to T cells, thus enhancing the infiltration and activation of T cells in the TME (38). However, cold tumors are very stubborn, and the immunosuppression in the TME is deeply rooted. The immunosuppressive cells, such as Tregs and MDSCs, inactivate the positive immunoregulatory cells and prevent their further infiltration (39). Therefore, it is necessary to increase the proportion of positive regulatory immune cells and, more importantly, to break the immunosuppression constructed by negative regulatory cells in the TME.

Based on the current clinical treatment status, besides the immunosuppression of the cold tumors, another major challenge for cancer immunotherapy is that immune-related adverse events often occurred during the systemic administration. With precise controllability, some activatable nanomedicines have been developed to improve the effectiveness and safety of clinical transformation of cancer immunotherapy (40). For example, an organic pronanostimulant was explored to combine photoactivatable immunostimulants with phototherapy and achieve synergistic precise immunoregulation with no obvious immune-related adverse effects (41). Moreover, some in situ formed bioresponsive nanomedicine could release the immunotherapeutic agents with a programmed activatable manner in the TME, thus awakening

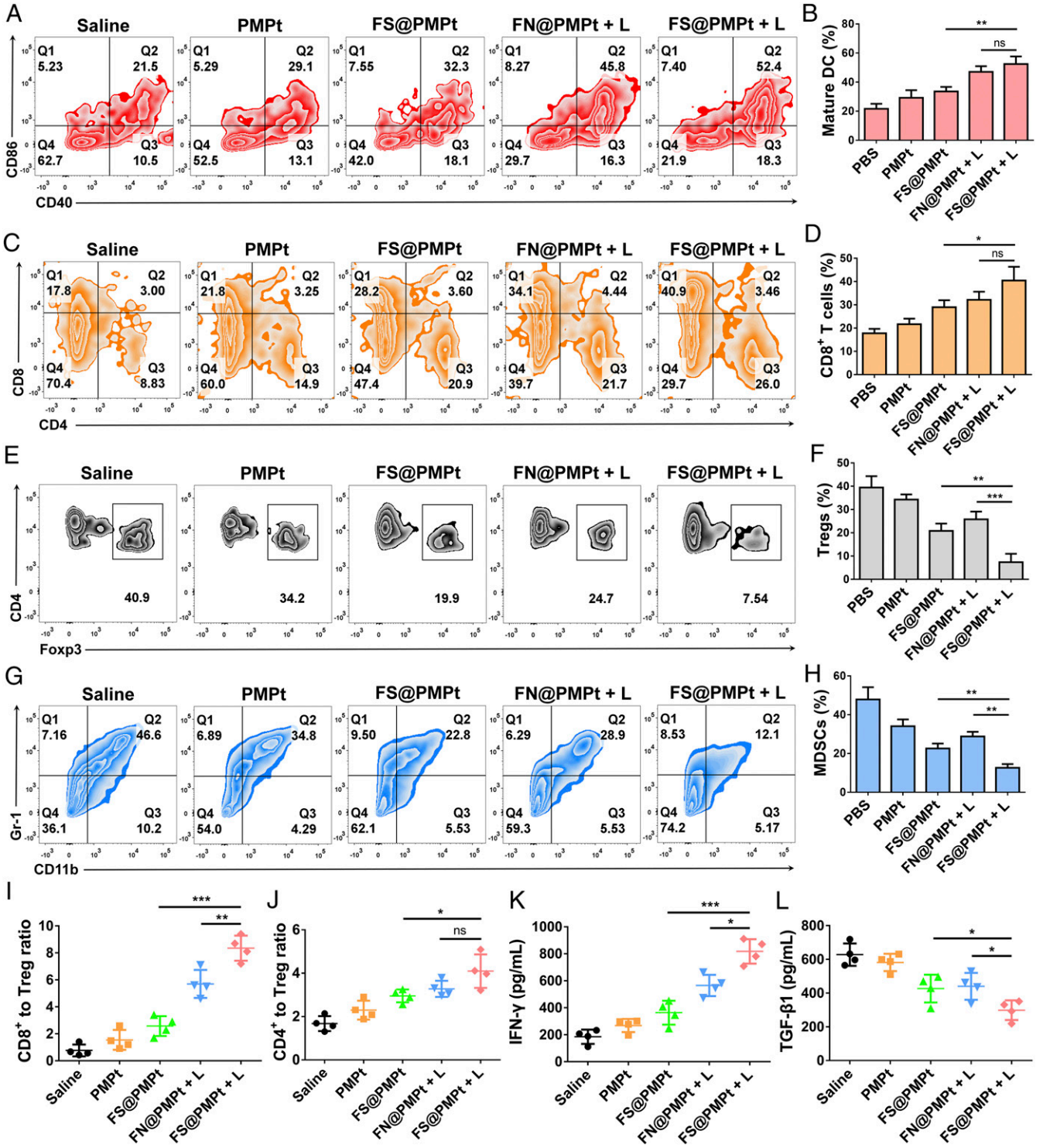

Fig. 6. Immune activation in vivo. (*A*) Flow cytometry assay and (*B*) quantitative analysis of DC maturation ($CD11c^+CD40^+CD86^+$) induced by different treatments on day 15 in the lymph nodes. Data represent mean ± SD ($n = 4$ biologically independent samples). (*C*) Flow cytometry assay and (*D*) quantitative analysis of $CD8^+$ T cell infiltration after different treatments on day 15 in the tumor. Data represent mean ± SD ($n = 4$ biologically independent samples). (*E*) Flow cytometry assay and (*F*) quantitative analysis of Tregs after different treatments on day 15 in the tumor. Data represent mean ± SD ($n = 4$ biologically independent samples). (*G*) Flow cytometry assay and (*H*) quantitative analysis of MDSCs after different treatments on day 15 in the tumor. Ratios of the tumor-infiltrating $CD8^+$ T cells (*I*) and $CD4^+$ T cells (*J*) to Tregs in the tumors upon different treatments. (*K*) IFN-γ and (*L*) TGF-β1 detected by ELISA in the TME after different treatments on day 15. Data represent mean ± SD ($n = 4$ biologically independent samples). *P* values were calculated by Student's *t* test, $^*P < 0.05$, $^{**}P < 0.01$, $^{***}P < 0.001$, ns = no significant difference.

both the innate and adaptive immunity with good biosafety and controllability, showing great potential for clinical treatment of tumor recurrence postsurgery (42, 43).

The FS@PMPt nanoclusters are also activatable nanomedicine with precise controllability and efficient immune regulation ability. Notably, the procedure and nanomodality in this work mainly bring

two inspirations to the clinical treatment of cancer immunotherapy. First, for the immunological cold tumors, drugs or treatments that could generate ICD should be combined with Tregs or MDSCs inhibitors to achieve synergistic immunoregulation and reverse immunosuppression. Second, precise activatable nanomedicines or nanomodalities could be developed to incorporate clinical combination strategies in a unified manner with superior biosafety and effectiveness.

Overall, in this study, we developed an immunomodulatory nanocluster FS@PMPt to reverse the immunosuppressive TME and turn a cold tumor into a hot tumor. FS@PMPt was assembled through F–F interaction with good stability and oxygen-carrying capacity to guarantee the production of sufficient ROS for potent ICD induction. Hence, the ICD induced by the nanocluster, accompanied by the exposure of CRT and release of ATP and HMGB1, promotes the maturation and antigen presentation of DCs both in vitro and in vivo. Also, significantly increased $CD8^+$ T cell infiltration was observed after the treatment of the nanocluster to further heat up the cold tumor and light the flames of the antitumor war. Meanwhile, the released PMPt prodrugs, working synergistically with the ICD induction, penetrated into the tumor to kill the Tregs and MDSCs, which are the main drivers of immunosuppression in a cold tumor. This immunomodulatory nanocluster FS@PMPt not only increased the infiltration of immunopositive cells from the outside but also decreased the immunosuppressive cells from the inside to break the shackles of immunosuppression in the TME, which provides a promising paradigm for improving the anti–cold tumor immunotherapy.

Materials and Methods

Experimental materials and methods for the synthesis, preparation, and characterization of the nanoclusters, immune activation, in vitro antitumor efficacy, and in vivo animal experiments are provided in *SI Appendix*. All animal experiments followed regulations of the Institutional Animal Care and Use Committee of China Pharmaceutical University, and protocols were approved by the Science and Technology Department of Jiangsu Province.

Data Availability. All study data are available in the article and *SI Appendix*.

ACKNOWLEDGMENTS. This work was supported by the National Key Research and Development Program of China (grant number: 2017YFA0205402), the Science Fund for Distinguished Young Scholars of Jiangsu Province, China (grant number: BK20170028), the Natural Science Foundation of Jiangsu Province (BK20180557), the China National Science Foundation (grant numbers: 81573377, 81872817, and 81803477), and the "Double First-Class" University Project of China Pharmaceutical University (grant number: CPU2018GY07).

1. J. H. Newman *et al*., Intratumoral injection of the seasonal flu shot converts immunologically cold tumors to hot and serves as an immunotherapy for cancer. *Proc. Natl. Acad. Sci. U.S.A.* **117**, 1119–1128 (2020).
2. N. Zaidi, E. M. Jaffee, Immune cells track hard-to-target brain tumours. *Nature* **565**, 170–171 (2019).
3. J. Li *et al*., Tumor cell-intrinsic factors underlie heterogeneity of immune cell infiltration and response to immunotherapy. *Immunity* **49**, 178–193.e7 (2018).
4. M. McLaughlin *et al*., Inflammatory microenvironment remodelling by tumour cells after radiotherapy. *Nat. Rev. Cancer* **20**, 203–217 (2020).
5. J. Galon, D. Bruni, Approaches to treat immune hot, altered and cold tumours with combination immunotherapies. *Nat. Rev. Drug Discov.* **18**, 197–218 (2019).
6. Z. Meng *et al*., Light-triggered in situ gelation to enable robust photodynamic-immunotherapy by repeated stimulations. *Adv. Mater.* **31**, e1900927 (2019).
7. X. Feng *et al*., Immunomodulatory nanosystems. *Adv. Sci. (Weinh.)* **6**, 1900101 (2019).
8. C. W. Ng, J. Li, K. Pu, Recent progresses in phototherapy-synergized cancer immunotherapy. *Adv. Funct. Mater.* **28**, 1804688 (2018).
9. C. Zhang *et al*., Enzyme-driven membrane-targeted chimeric peptide for enhanced tumor photodynamic immunotherapy. *ACS Nano* **13**, 11249–11262 (2019).
10. R. Liang *et al*., Oxygen-boosted immunogenic photodynamic therapy with gold nanocages@manganese dioxide to inhibit tumor growth and metastases. *Biomaterials* **177**, 149–160 (2018).
11. S. Musetti, L. Huang, Nanoparticle-mediated remodeling of the tumor microenvironment to enhance immunotherapy. *ACS Nano* **12**, 11740–11755 (2018).
12. M. P. Matheu *et al*., Imaging regulatory T cell dynamics and CTLA4-mediated suppression of T cell priming. *Nat. Commun.* **6**, 6219 (2015).
13. P. Pandiyan, L. Zheng, S. Ishihara, J. Reed, M. J. Lenardo, CD4+CD25+Foxp3+ regulatory T cells induce cytokine deprivation-mediated apoptosis of effector CD4+ T cells. *Nat. Immunol.* **8**, 1353–1362 (2007).
14. L. Wang *et al*., Connecting blood and intratumoral T_{reg} cell activity in predicting future relapse in breast cancer. *Nat. Immunol.* **20**, 1220–1230 (2019).
15. H. Wang, F. Franco, P. C. Ho, Metabolic regulation of Tregs in cancer: Opportunities for immunotherapy. *Trends Cancer* **3**, 583–592 (2017).
16. Y. Mi, C. T. Hagan IV, B. G. Vincent, A. Z. Wang, Emerging nano-/microapproaches for cancer immunotherapy. *Adv. Sci. (Weinh.)* **6**, 1801847 (2019).
17. A. Facciabene, G. T. Motz, G. Coukos, T-regulatory cells: Key players in tumor immune escape and angiogenesis. *Cancer Res.* **72**, 2162–2171 (2012).
18. X. R. Ros, L. Vermeulen, Turning cold tumors hot by blocking TGF-β. *Trends Cancer* **4**, 335–337 (2018).
19. N. Kamran *et al*., Immunosuppressive myeloid cells' blockade in the glioma microenvironment enhances the efficacy of immune-stimulatory gene therapy. *Mol. Ther.* **25**, 232–248 (2017).
20. A. R. de Biasi, J. Villena-Vargas, P. S. Adusumilli, Cisplatin-induced antitumor immunomodulation: A review of preclinical and clinical evidence. *Clin. Cancer Res.* **20**, 5384–5391 (2014).
21. C. W. Tseng *et al*., Pretreatment with cisplatin enhances E7-specific CD8+ T-cell-mediated antitumor immunity induced by DNA vaccination. *Clin. Cancer Res.* **14**, 3185–3192 (2008).
22. C. L. Chang *et al*., Dose-dense chemotherapy improves mechanisms of antitumor immune response. *Cancer Res.* **73**, 119–127 (2013).
23. J. Guo, Z. Yu, M. Das, L. Huang, Nano codelivery of oxaliplatin and folinic acid achieves synergistic chemo-immunotherapy with 5-fluorouracil for colorectal cancer and liver metastasis. *ACS Nano* **14**, 5075–5089 (2020).
24. Q. Song *et al*., Tumor microenvironment responsive nanogel for the combinatorial antitumor effect of chemotherapy and immunotherapy. *Nano Lett.* **17**, 6366–6375 (2017).
25. P. Yu *et al*., Artificial red blood cells constructed by replacing heme with perfluorodecalin for hypoxia-induced radioresistance. *Adv. Ther.* **2**, 1900031 (2019).
26. Z. Zhou *et al*., Perfluorocarbon nanoparticle-mediated platelet inhibition promotes intratumoral infiltration of T cells and boosts immunotherapy. *Proc. Natl. Acad. Sci. U.S.A.* **116**, 11972–11977 (2019).
27. W. L. Liu *et al*., Expandable immunotherapeutic nanoplatforms engineered from cytomembranes of hybrid cells derived from cancer and dendritic cells. *Adv. Mater.* **31**, e1900499 (2019).
28. Z. Wang *et al*., Janus nanobullets combine photodynamic therapy and magnetic hyperthermia to potentiate synergetic anti-metastatic immunotherapy. *Adv. Sci. (Weinh.)* **6**, 1901690 (2019).
29. G. Chen *et al*., Reversibly stabilized polycation nanoparticles for combination treatment of early- and late-stage metastatic breast cancer. *ACS Nano* **12**, 6620–6636 (2018).
30. R. Kuai *et al*., Elimination of established tumors with nanodisc-based combination chemoimmunotherapy. *Sci. Adv.* **4**, eaao1736 (2018).
31. N. Kanaya *et al*., Immune modulation by telomerase-specific oncolytic adenovirus synergistically enhances antitumor efficacy with anti-PD1 antibody. *Mol. Ther.* **28**, 794–804 (2020).
32. D. Ha *et al*., Differential control of human Treg and effector T cells in tumor immunity by Fc-engineered anti-CTLA-4 antibody. *Proc. Natl. Acad. Sci. U.S.A.* **116**, 609–618 (2019).
33. P. Zhang *et al*., Therapeutic targeting of tumor-associated myeloid cells synergizes with radiation therapy for glioblastoma. *Proc. Natl. Acad. Sci. U.S.A.* **116**, 23714–23723 (2019).
34. D. V. F. Tauriello *et al*., TGFβ drives immune evasion in genetically reconstituted colon cancer metastasis. *Nature* **554**, 538–543 (2018).
35. S. Mariathasan *et al*., TGFβ attenuates tumour response to PD-L1 blockade by contributing to exclusion of T cells. *Nature* **554**, 544–548 (2018).
36. Z. Li *et al*., Targeting pulmonary tumor microenvironment with CXCR4-inhibiting nanocomplex to enhance anti-PD-L1 immunotherapy. *Sci. Adv.* **6**, eaaz9240 (2020).
37. A. Mansurov *et al*., Collagen-binding IL-12 enhances tumour inflammation and drives the complete remission of established immunologically cold mouse tumours. *Nat. Biomed. Eng.* **4**, 531–543 (2020).
38. A. D. Garg *et al*., Dendritic cell vaccines based on immunogenic cell death elicit danger signals and T cell-driven rejection of high-grade glioma. *Sci. Transl. Med.* **8**, 328ra27 (2016).
39. M. D. Sharma *et al*., The PTEN pathway in Tregs is a critical driver of the suppressive tumor microenvironment. *Sci. Adv.* **1**, e1500845 (2015).
40. C. Zhang, K. Pu, Molecular and nanoengineering approaches towards activatable cancer immunotherapy. *Chem. Soc. Rev.* **49**, 4234–4253 (2020).
41. J. Li *et al*., Organic semiconducting pro-nanostimulants for near-infrared photoactivatable cancer immunotherapy. *Angew. Chem. Int. Ed. Engl.* **58**, 12680–12687 (2019).
42. C. Wang *et al*., In situ formed reactive oxygen species-responsive scaffold with gemcitabine and checkpoint inhibitor for combination therapy. *Sci. Transl. Med.* **10**, eaan3682 (2018).
43. Q. Chen *et al*., In situ sprayed bioresponsive immunotherapeutic gel for post-surgical cancer treatment. *Nat. Nanotechnol.* **14**, 89–97 (2019).